Dyes and Pigments 187 (2021) 109093

Contents lists available at ScienceDirect

Dyes and Pigments

journal homepage: http://www.elsevier.com/locate/dyepig

The effect of benzoxazole unit on the properties of cyclic thiourea functionalized triphenylamine dye sensitizers

Shuang Liu [a], Muhan Zhou [a], Guanjun Zhang [a], Ran Chen [a], Pengjuan Zhou [a], Zhongwei An [a,c,*], Xinbing Chen [a], Qi An [b], Pei Chen [a]

[a] Key Laboratory of Applied Surface and Colloid Chemistry (MOE), Shaanxi Key Laboratory for Advanced Energy Devices, Shaanxi Engineering Laboratory for Advanced Energy Technology, School of Materials Science and Engineering, Shannxi Normal University, Xi'an, 710062, China
[b] North Institute of Scientific and Technical Information, Beijing, 100089, China
[c] Xi'an Modern Chemistry Research Institute, Xi'an, 710065, China

ARTICLE INFO

Keywords:
Dye-sensitized solar cells
Benzoxazole
D-π-A-A
Dipole moment
Dye sensitizer

ABSTRACT

Two D-π-A-A sensitizers (**AZ6-B20** and **AZ6-B21**) were synthesized by inserting the benzoxazole group as an auxiliary acceptor between the π-linker and the acceptor. And a D-A-π-A sensitizer (**AZ6-B19**) was also synthesized in our previous works by the insertion of the benzoxazole between the donor and the π-linker. The effects of benzoxazole groups on the properties at different sites of dye sensitizers were distinguishing. Their light harvest abilities were investigated by UV–vis spectra both in the solution and on the films. The results show that the absorption bands of UV–vis spectra are quite different from D-A-π-A and D-π-A-A dyes. The much more intensive molar extinction coefficients (53807 $M^{-1}cm^{-1}$ and 52555 $M^{-1}cm^{-1}$) were observed at around 575 nm for D-π-A-A dyes. The photovoltaic properties of DSSCs were also evaluated by *J-V* curves and IPCE measurements. The results confirmed that D-π-A-A dyes delivered high photovoltaic efficiency (**AZ6-B20**: 7.48%, **AZ6-B21**: 8.67%) compared with that of D-A-π-A dye (**AZ6-B19**: 3.27%). The details on the relation of the structures/properties were discussed by the optical physical absorption, electrical chemical measurements and DFT calculations.

1. Introduction

The energy demand and the environmental pollution are the most important issues to be faced in human society, which have drawn scientist's attention to new energy sources [1]. It is a feasible strategy that the traditional fossil fuels could be replaced by the cheap and renewable clean energy [2]. Solar energy is widely concerned with its advantages of inexhaustible, clean and environmental friendly [3,4]. In comparison with conventional silicon solar cells, it is considered that DSSCs is one of the most hopeful new-energy devices owing to the advantages of low cost, simple fabrication process and good photoelectric efficiency [5,6]. Since it was reported by O′ Regan and Gratzel in 1991 [7], the PCE of DSSCs has been gone up from 7.1% to 14.3% [8]. In general, DSSCs requires four major components: dye sensitizer, counter electrode, electrolyte, and semiconductor [9]. Although the variation of each component in DSSCs would result in an influence on the PCE [10], the more important component of DSSCs is the sensitizer which plays a very crucial role in harvesting the sunlight and resulting photo-electron. For many years, Ruthenium (Ru) based metal complex dyes such as N719 [11], Z907 [12], N749 [13] and N3 [14] have shown remarkable efficiency under sunlight due to their excellent absorption in visible region and stability. Nevertheless, the dyes have remained defective at many points on rarity of Ru metal, pollution of the environment, and less molar extinction coefficients [15]. In recent years, metal-free organic dyes are regarded as an attractive alternative because their advantages of low cost, high molar extinction coefficient and the structure versatility [16,17].

Efficient metal-free organic sensitizers are characterized by"donor-π linker-acceptor (D-π-A)" structures in which the modification of every part plays a significant improvement of the photovoltaic performance [18], especially incorporating an auxiliary acceptor is beneficial for extending the absorption spectrum. A wide variety of organic dyes with typical auxiliary acceptor such as benzothiazole [19], benzotriazole [20] and difluorobenzo[c] [1,2,5]thiadiazole [21], spiro[fluorene-9,

* Corresponding author. Key Laboratory of Applied Surface and Colloid Chemistry, School of Materials Science and Engineering, Shannxi Normal University, Xi'an, 710062, China.
E-mail address: gmecazw@163.com (Z. An).

https://doi.org/10.1016/j.dyepig.2020.109093
Received 12 September 2020; Received in revised form 15 December 2020; Accepted 15 December 2020
Available online 25 December 2020

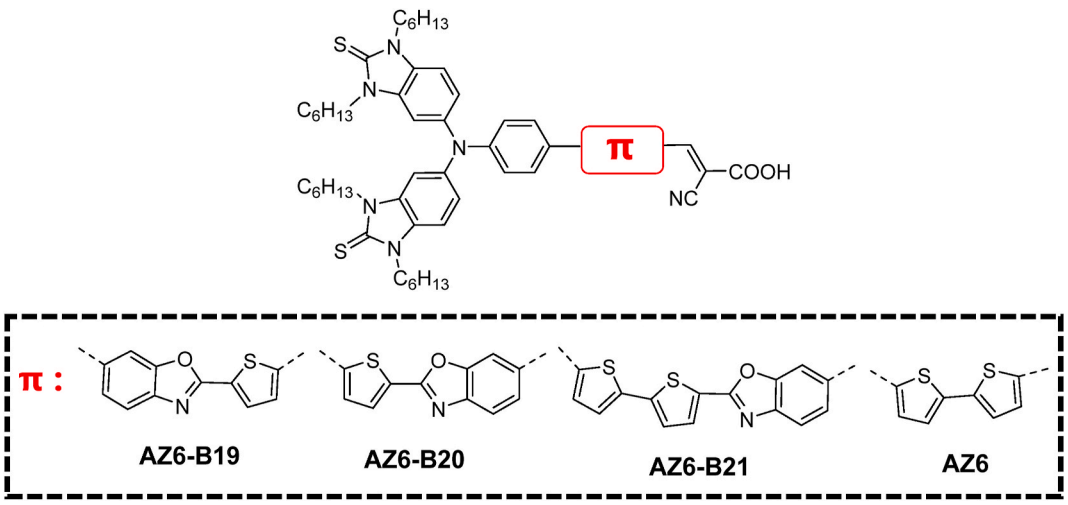

Fig. 1. Chemical structures of the dyes. Herein C_6H_{13} denotes *n*-hexyl.

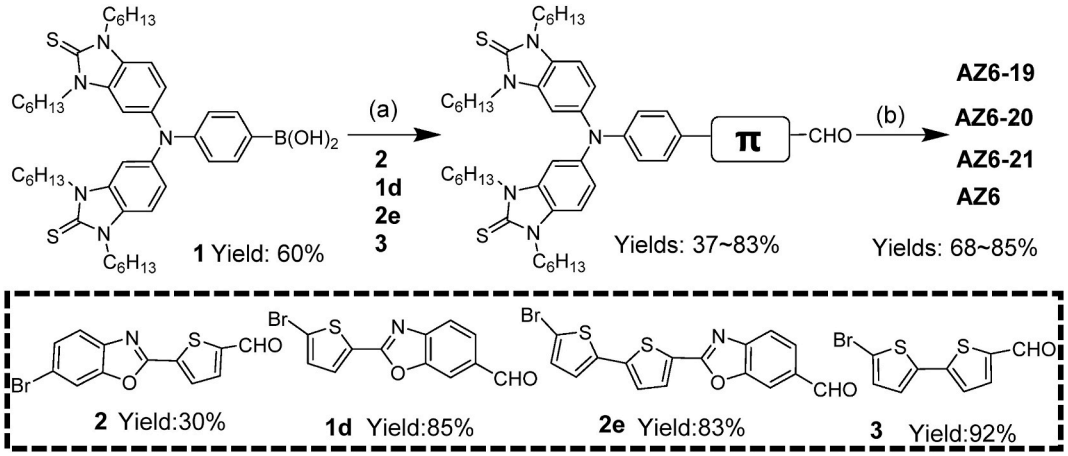

Fig. 2. Synthetic routes of **AZ6-B19**, **AZ6-B20**, **AZ6-B21** and **AZ6**. *Reaction conditions*: (a) K_2CO_3 aqueous solution, $Pd(PPh_3)_4$, TBAB, DMF, 75 °C, 2 h; (b) cyanoacetic acid, piperidine, CH_3COOH, 75 °C, 5 h.

9′-phenanthren]-10′-one [22] have been reported to be excellent dyes with good photon conversion efficiency. However, recent literatures revealed that the introduction of difluorobenzo[c] [1,2,5]thiadiazole (DFBT) as an auxiliary acceptor results a narrow absorption range and high molar extinction coefficient [23]. Meanwhile, the UV–vis absorption behavior of dyes in solution and on TiO_2 films is often different. Normally, the absorption spectrum on the film is red-shifted compared to that in solution [24–26], and another exception is found that the absorption spectrum is blue-shifted on the TiO_2 film [27]. All of the dye sensitizers with an auxiliary acceptor can strengthen the absorption intensity, thereby to increase the light harvesting ability. However it is necessary to further understand that which part of the molecule to be inserted by an auxiliary acceptor is an effective way to achieve the optimum properties.

In this study, based on our former report of the organic dyes with the cyclic thiourea functionalized triphenylamine as a donor [28], We chosen electron-withdrawing benzoxazole unit as the auxiliary acceptor in our feature molecule **AZ6**, and get a D-π-A-A dyes (**AZ6-B20** and **AZ6-B21**). The Comparison D-A-π-A dye **(AZ6-B19)** was synthesized in our previous works (**AZ6-B19**, **AZ6-B20** and **AZ6-B21** of Fig. 1) [29]. The two D-π-A-A dyes show wider spectral absorption range and better photon conversion efficiency (**AZ6-B19**: 3.27%, **AZ6-B20**: 7.48% and **AZ6-B21**: 8.67%). The optimal geometry structure of the dyes were obtained by density functional theory (DFT) calculations, and the photophysical absorption, electrochemical measurement and photovoltaic performance were correlated.

2. Experimental section

2.1. Materials & synthesis

Unless otherwise noted, all chemicals were commercially available and used as received. (4-(bis(1,3-dihexul-2-thioxo-2,3-dihydro-1H-benzo[d]imidazole-5-yl) amino) phenyl) boronic acid (**1**) was reported in our previous paper [28]. **AZ6-B19** was synthesized in our previous work. The synthetic routes to the new dyes **AZ6-B20**, **AZ6-B21** are shown in Fig. 2, and the aldehyde compounds **2b**, **2c**, **3b** and **3c** can be found in the Supporting information. All the chemicals and solvents used in this work were of analytical grade and used without further purification unless otherwise stated.

2.2. Structure confirmation

^1H NMR and ^{13}C NMR spectra were recorded on JEOL-400MHz and JEOL-600MHz instruments with tetramethylsilane (TMS) as the internal standard. Data of ^1H NMR and ^{13}C NMR were recorded in $CDCl_3$ or DMSO-d_6 solution. Matrix-assisted laser desorption ionization time of flight mass spectra (MALDI-TOF-MS) and High resolution mass spectra

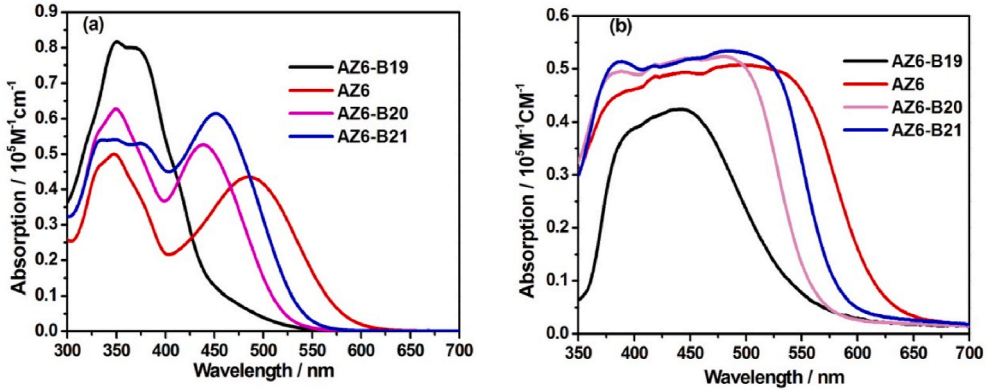

Fig. 3. UV–Vis absorption spectra of the dyes in MeCN-DCM (1:1, v/v) solution(a) and on TiO_2 films (b). The absorption of a TiO_2 film has been subtracted for clarity of presentation.

Table 1
The optical properties of the dyes.

Dye	λ^amax/nm	$\varepsilon^a/M^{-1}cm^{-1}$	λ^bmax/nm	$\varepsilon^b/M^{-1}cm^{-1}$	λ^{PL}max/nm	Stokes shift/cm^{-1}
AZ6-B20	438	52423	482	52555	575	5440
AZ6-B21	451	59400	487	53807	574	4812
AZ6-B19	365	56300	442	42446	436	4461
AZ6	485	42790	509	50085	576	3197

[a] Absorption and PL spectra were measured in MeCN/DCM solutions (1×10^{-5} M).
[b] Maximum absorption spectra was measured on sensitized TiO_2 films.

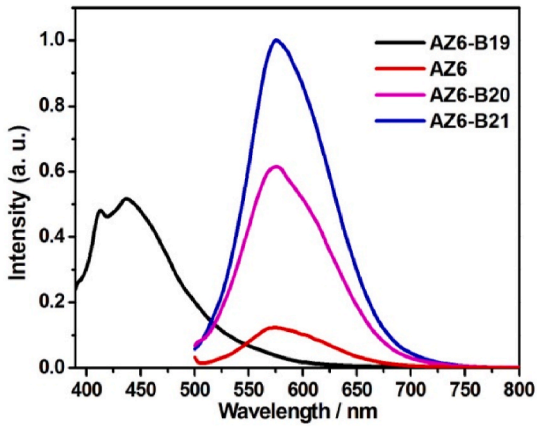

Fig. 4. The fluorescence emission spectra of the dyes in MeCN/DCM (1:1, v/v) solution.

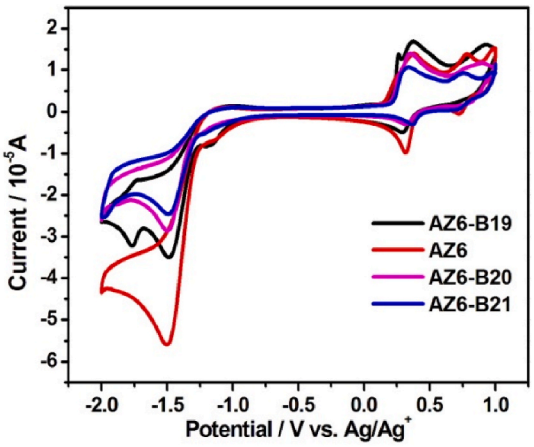

Fig. 5. Cyclic voltammograms of the dyes in MeCN-DCM (1:1, v/v) solution.

(HRMS) were measured with a Bruker mass spectrometer. The infrared spectra was measured by a fourier infrared spectrometer from the German Bruker company. The elemental analyzer was a Vario EL III model produced by the German element analysis system company.

2.3. Photophysical measurements

2.3.1. UV–Vis absorption spectra

UV–Vis absorption spectra of the dyes in MeCN-DCM (1:1, v/v, where MeCN is acetonitrile, and DCM is dichloromethane; 1×10^{-5} M) solutions and on the adsorbed TiO_2 films were measured with a Shimadzu UV-3600 spectrophotometer in Japan. The absorption spectra are shown in Fig. 3, and the corresponding photophysical data are listed in Table 1.

2.3.2. The PL spectra

The PL spectra of the dyes were measured in MeCN-DCM (1:1, v/v; 1×10^{-5} M) solutions. And the Shimadzu F-7000 PL spectrophotometer was made in Japan. The PL spectra of the dyes are shown in Fig. 4, and the corresponding photophysical data are also listed in Table 1.

2.4. Electrochemical properties

The CV were conducted on a CH1604D Electrochemical Workstation at a scan rate 100 mV s^{-1}, measured in MeCN/DCM (1/1, v/v) solutions containing 0.1 M tetrabutylammonium hexyaflurophosphate (Bu_4NPF_6) under nitrogen atmosphere, and carried out in a typical three-electrode electrochemical system (working electrode: glassy carbon; counter electrode: Pt; reference electrode: Ag/Ag^+). The redox potential were calibrated with ferrocene/ferrocenium (Fc/Fc^+) as the internal reference. Energies of HOMO and LUMO could be derived by the formulas of $E_{HOMO} = -e\ (\phi_{ox} + 4.71)$ (eV), and $E_{LUMO} = -e\ (\phi_{red} + 4.71)$ (eV); $E_g^{ec} = e\ (\phi_{ox} - \phi_{red})$ (eV).

The CV curves of the dyes are shown in Fig. 5, and the

Table 2
The electrochemical data of the dyes.

Dye	ϕ_{ox}/V	ϕ_{red}/V	E^{a}_{HOMO}/eV	E^{b}_{LUMO}/eV	$E^{c}_{0\text{-}0}$/eV
AZ6-B20	0.21	−1.31	−4.92	−3.40	1.52
AZ6-B21	0.22	−1.27	−4.93	−3.44	1.49
AZ6-B19	0.21	−1.04	−4.92	−3.67	1.25
AZ6	0.16	−1.26	−4.87	−3.45	1.42

[a] The oxidation potential ϕ_{ox} in MeCN/DCM solutions was determined from cyclic voltammograms and used to describe the ground-state energy HOMO.
[b] E_{LUMO} was calculated from E_{ox}–$E_{0\text{-}0}$.
[c] $E_{0\text{-}0}$ was calculated from $E_{0\text{-}0} = 1240/\lambda_{int}$ and λ_{int} was the intersection of the normalized absorption and emission spectra.

electrochemical data are listed in Table 2.

2.5. Theoretical calculation

Full geometry optimizations have been carried out without imposing any constraints using the Gaussian 09 program package. Spin-restricted DFT calculations were carried out in the framework of the generalized gradient approximation (GGA) using the B3LYP exchange–correlation functional and the 6-311G (d, p) basis set. The optimal configuration of dye molecules are shown in Fig. 6 and the corresponding data are summarized in Table 3.

2.6. Fabrication and characterization of DSSCs

TiO_2 film photo anode was purchased from Yingkou OPV Tech new energy company. It consisted of 20 nm, 200 nm and 400 nm TiO_2 film (0.5 cm*0.5 cm), which was immersed in a 0.4 mM dye sensitized solution (DCM/t-BuOH = 1/1, v/v) under darkfor 24 h at room temperature. The photovoltaic characteristics of dyes were obtained with typical sandwich cells using an electrolyte composed of 0.12 M I_2, 0.1 M LiI, 1.0 M DMPII and 0.5 M 4-TBP in CH_3CN/3-mPn (1/3, v/v) solution. All other fabrication processes of DSSCs were also performed according to the published method [30].

Photocurrent-voltage (*J-V*) characteristics of the DSSCs were measured under illumination with AM 1.5 G solar light from a 300 W xenon lamp solar simulator (94022A, Newport Co., USA). The incident light intensity was calibrated to 100 mW cm^{-2} with a standard silicon solar cell. *J-V* characteristics were recorded with a digital source meter (Keithley 2400) controlled by a computer. The action spectra of monochromatic incident photon-to-current conversion efficiency (IPCE) for solar cells were tested on a commercial setup (QTest Station 2000 IPCE Measurement System, Crowntech, USA).

Electrical impedance spectra (EIS) under dark conditions with bias −0.7 V were also measured with CH1604D Electrochemical Workstation at frequencies of 0.05–100000 Hz. The magnitude of the alternative

Table 3
HOMO/LUMO levels, dihedral angle and dipole moment data of the dyes.

Dye	AZ6-B19	AZ6-B20	AZ6-B21	AZ6
θ_1/°	38.63	24.18	25.90	25.36
θ_2/°	/	/	18.53	15.01
θ_3/°	0.36	0.68	0.43	/
E_{HOMO}/eV	−5.24	−5.32	−5.24	−5.26
E_{LUMO}/eV	−3.21	−2.91	−2.96	−2.97
E_g/eV	1.80	2.41	2.28	2.29
Dipole moment/Debye	4.1856	6.2842	7.1719	4.9313

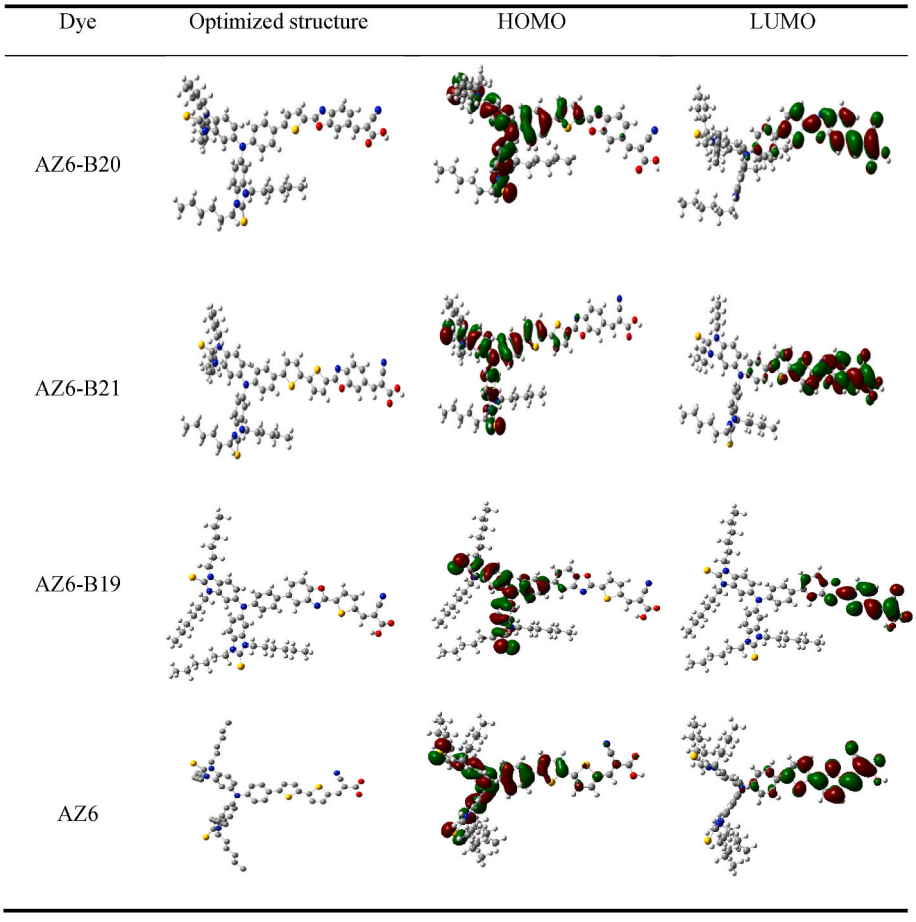

Fig. 6. The frontier orbitals and energy levels of the dyes by DFT calculations.

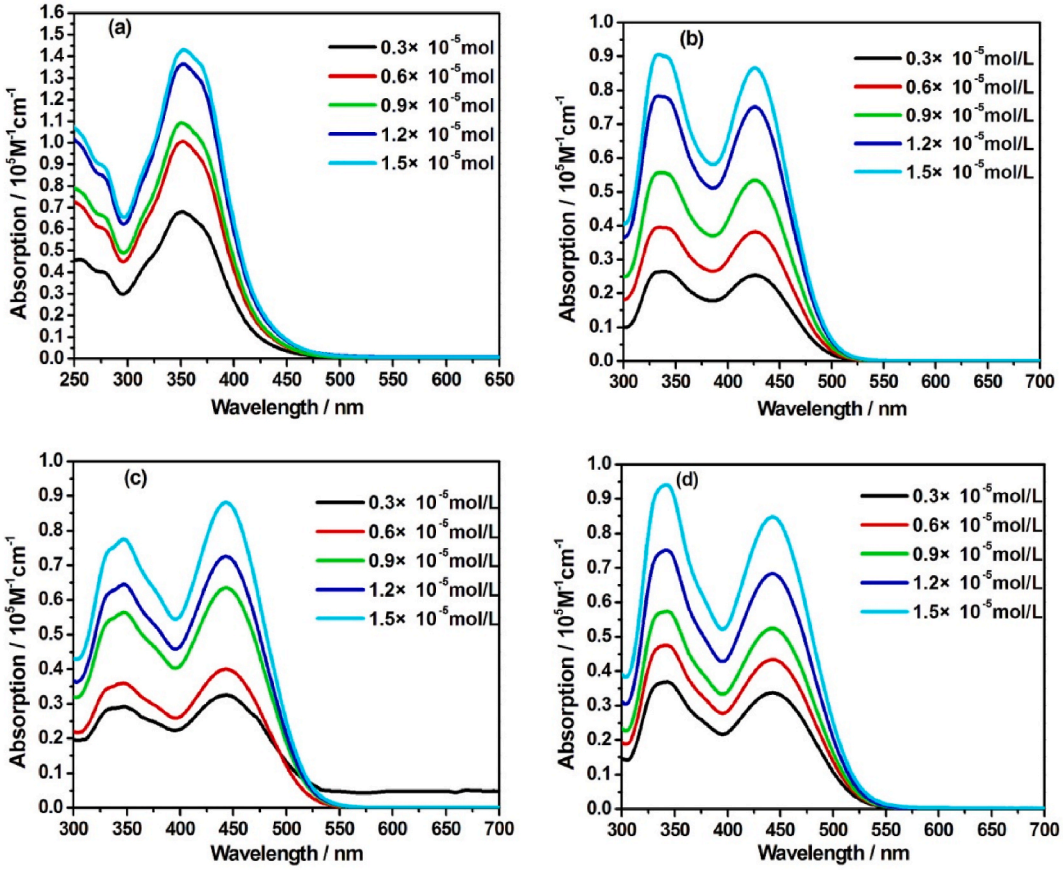

Fig. 7. The UV–vis absorption spectra of (a) **AZ6-B19**, (b) **AZ6-B20**, (c) **AZ6-B21** and (d) AZ6 in 0.01 g mL^{-1} NaOH solution ($H_2O/CH_3CH_2OH/THF = 1/1/1$, v/v/v) for various concentration.

signal was 10 mV. Charge-transfer resistances were determined by fitting the impedance spectra using Z-view software.

2.7. The capacity of DSSCs

Dye sensitizers were prepared into solutions with different concentration gradients to measure their UV–vis absorption spectra in Fig. 7. Then the standard curve equation is obtained by linear fitting in Fig. 8.

The photo anode loaded with dye sensitizer was immersed in 7 mL sodium hydroxide solution (0.01 mg/L) for 12 h, and the UV–vis absorption value of the solution was measured in Fig. 9. Then capacity of the dyes can be calculated by combining the standard equation (as Fig. 10) and the battery area, and the data is shown in Table 4.

3. Results and discussion

3.1. Synthesis and structural characterization

The synthetic approach to sensitizers **AZ6-B20** and **AZ6-B21** starting from the corresponding cyclic thiourea triphenylamine is depicted in Fig. 2. The compound **2b** was synthesized by cyclization, reduction and bromination reactions. The compound **2c** was synthesized in a similar way as the preparation of **2b**. The two dyes (**AZ6-B20**, **AZ6-B21**) were synthesized by Suzuki cross-coupling and Knoevenagel condensation reactions. Suzuki cross-coupling of compound **1** and bromide **2b**/**2c** produced the corresponding aldehydes **3b**/**3c**. The target dyes were obtained via Knoevenagel condensation reaction of aldehydes (**3b**, **3c**) and cyanoacetic acid. Their structures were confirmed by ^1H NMR, ^{13}C NMR spectroscopy, mass spectroscopy, infrared spectroscopy and elemental analysis.

3.2. Optical properties

As shown in Fig. 3, the dyes **AZ6-B20**, **AZ6-B21** and **AZ6** exhibit two distinct absorption bands. As reported in Refs. [31,32], the absorption bands in the high-energy region (300–400 nm) was attributed to localized aromatic π-π* transitions, whereas the least energetic absorption bands in the visible region (400–600 nm) can be assigned to an intra-molecular charge-transfer (ICT) process between the cyclic thiourea functionalized triphenylamine donor unit to the cyanoacrylic acid acceptor. After the insertion of the benzoxazole group between the donor and the thienyl spacer, the ICT absorption band of the dye **AZ6-B19** was remarkably blue-shifted, this was attributed to the lower transition probability (Fig. 6). The increase of the maximum absorption and the red-shift of the maximum absorption of **AZ6-B21** compared to that of **AZ6-B20** can be explained by the enhanced electron delocalization over thienyl spacers of increasing lengths. The same phenomenon has been observed for other organic dyes when the π-conjugation of the spacers is extended [32]. Compared with **AZ6**, **AZ6-B21** exhibited a blue-shifting of 34 nm in the maximum absorption wavelength (λ_{max}), which could be attributed to large steric effect due to the insertion of benzoxazole group (Table 3). While its molar extinction coefficients (59400 $M^{-1}cm^{-1}$) are higher than that of **AZ6** (42790 $M^{-1}cm^{-1}$), which is beneficial for good light harvesting ability.

The absorption wavelengths of all the dyes on TiO_2 films are widened, which is due to the interaction of the anchoring groups with the TiO_2 surface and J-aggregation of photosensitizer molecules [33,34]. The increased delocalization of the π* orbital of the conjugated skeleton was caused by the interaction between the carboxylate group and the Ti^{4+} ions, and the energy of the π* level is directly decreased. This is beneficial for harvesting the visible light. In fact, the geometric

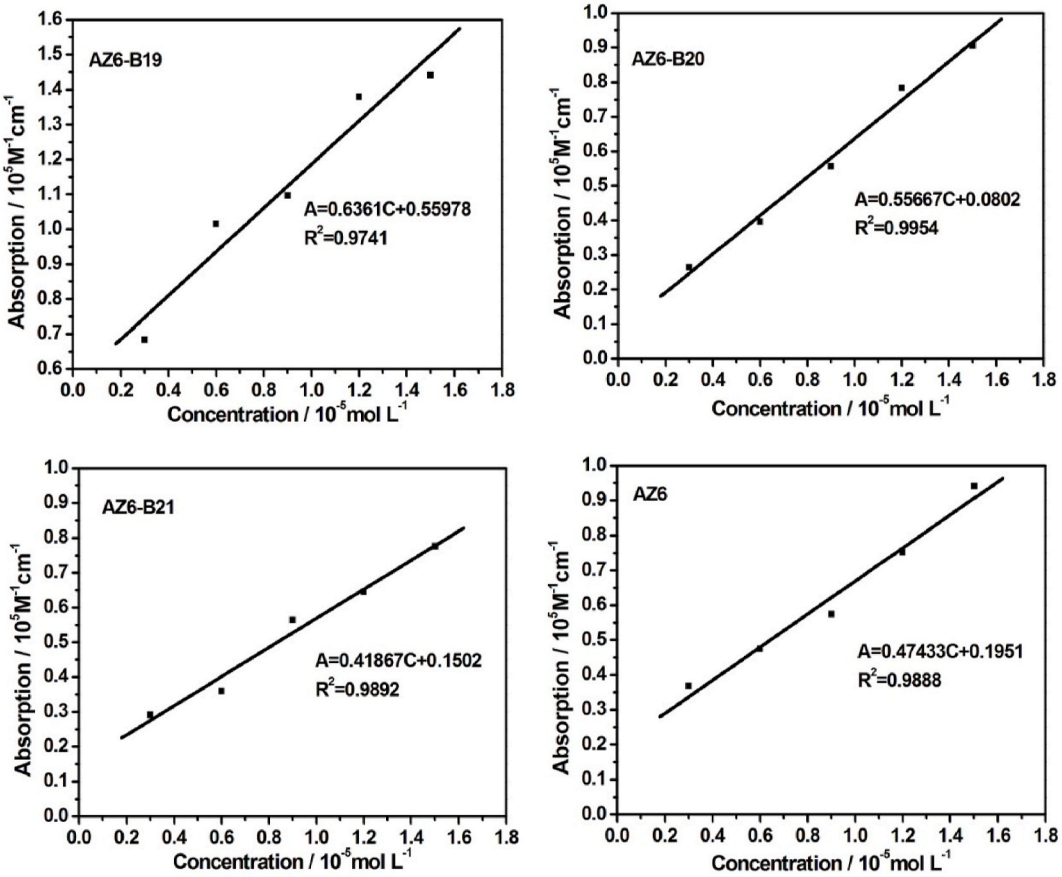

Fig. 8. The C-A fitting linear of **AZ6-B19**, **AZ6-B20**, **AZ6-B21** and **AZ6**.

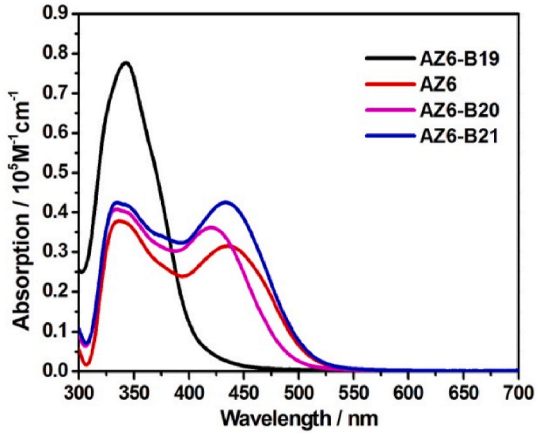

Fig. 9. The UV–vis absorption spectra of the eluted **AZ6-B19**, **AZ6**, **AZ6-B20** and **AZ6-B21** in 7 mL 0.01 g mL^{-1} NaOH solution.

packing of dye would play a very important role to extend the absorption range. For example, the dihedral angle of dye **AZ6-B20** (24.18°) is smaller than that of **AZ6** (25.36°), hence the steric effect of molecule **AZ6** is large. When the dye sensitizers are loaded on the TiO_2 film, compared with the more distorted molecular structure of **AZ6**, **AZ6-B20** is expected to improve the overlap between the HOMO level to the LUMO level. Therefore, the larger overlap in **AZ6-B20** translates into a higher transition probability, resulting in a higher molar extinction coefficient (Fig. 3b). In addition, the dihedral angle between two π-linkers in **AZ6** and **AZ6-B20** are 15.01 and 0.68, respectively. This is to say, the relative volume of the molecules **AZ6-B20** is smaller than **AZ6**, therefore there is more loading probability on the TiO_2 surface, further resulting in a larger dye-loading capacity than **AZ6** (Table 4).

The maximum emission band locates at 575 nm for **AZ6-B20**, 574 nm for **AZ6-B21**, 436 nm for **AZ6-B19** and 576 nm for **AZ6**, respectively. Large Stokes shift (3197-5440 cm^{-1}) can be observed in all the dyes, which is attributed to the charge transfer nature of the excited state.

3.3. Electrochemical properties

It is well-known that the energy levels of sensitizers need to match the energy levels of the redox potential of iodine/iodide electrolyte and the conduction-band-edge energy level of the TiO_2 electrode. As shown in Table 2, the HOMO energy levels of the dyes are −4.92 eV, −4.93 eV and −4.87 eV respectively, which are lower than the redox potential of iodine/iodide electrolyte (−4.0 eV), meaning that the designed dyes have potential to obtain electrons from electrode to regenerate the dye molecules. The LUMO energy levels are more positive than the conduction band (CB) of TiO_2 level (−4.7 eV), which means that excited electrons can be injected into TiO_2 CB effectively.

Generally, the energy gap between HOMO and LUMO energy level affects the photoelectron transition from the dye molecules to the TiO_2 conduction band. The narrower energy gap is favorable for such a transition. The HOMO and LUMO energy gaps of the dyes are 1.52 eV for **AZ6-B20**, 1.49 eV for **AZ6-B21** and 1.42 eV for **AZ6**, which is smaller than energy gaps calculated, which are consistent with their optical absorption properties.

3.4. Theoretical approach

The B3LYP/6–311G (d, p) level of theory was carried out to gain further insight into the electronic distribution of the frontier molecular

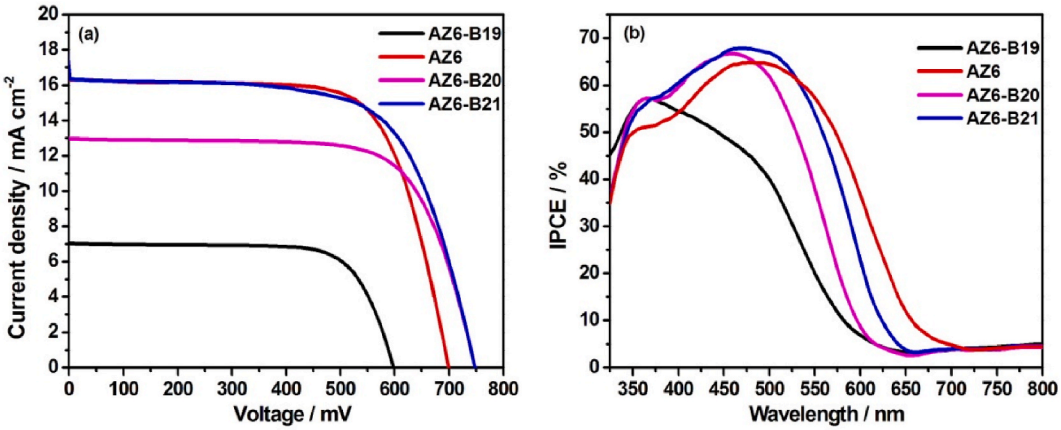

Fig. 10. *J-V* characteristics (a) and IPCE spectra (b) of DSSCs based on **AZ6-B19**, **AZ6**, **AZ6-B20** and **AZ6-B21**.

Table 4
The capacity data of the dyes.

Dye	λ_{max}/nm	C/10^{-5}M L^{-1}	Capacity/10^{-7}M cm^{-2}
AZ6-B20	334	0.59	1.65
AZ6-B21	336	0.65	1.82
AZ6-B19	343	0.35	0.98
AZ6	337	0.39	1.09

Table 5
The photovoltaic performance data of dyes.

Dye	J_{sc}/mA cm^{-2}	V_{oc}/mV	FF	PCE/%	IPCE/%(λ_{max}/nm)
AZ6-B21	13.92	749.5	0.79	8.22	67.86(470)
AZ6-B20	12.96	750.0	0.72	6.99	66.74(460)
AZ6-B19	7.02	601.8	0.76	3.19	57.26(365)
AZ6	16.32	699.0	0.71	8.05	64.85(480)

orbitals and the molecular structures for these sensitizers. The results are presented in Table 3. The dihedral angles between the donors and the π-bridge of the dyes **AZ6-B20**, **AZ6-B21**, and **AZ6** are 24.18°, 25.90°, and 25.36° respectively, this larger deformation may be due to the spatial repulsion caused by the interaction between the hydrogen on phenyl and the large sulfur atom on the thiophene ring. Meanwhile, the dihedral angle of **AZ6-B19** is 38.63°, due to the repulsion of nitrogen and oxygen heteroatoms on the benzoazole group. In terms of the overall geometry of the dye **AZ6-B19** molecules, the dye molecules with the benzoxazole group have a more distorted structure, which is not conducive for dye molecules to overlap with each other and contact between conduction band surface and electrolyte, further inhibiting π-π accumulation and dye composite within the molecule [35].

The dipole moments (Debye) of **AZ6-B20** (6.2842) and **AZ6-B21** (7.1719) are bigger than that of **AZ6** (4.9313), which show that the benzoxazole group as auxiliary acceptor increases the polarity of the dye molecule. Meanwhile, the dipole moment (Debye) of **AZ6-B19** (4.1856) is less than that of **AZ6** (4.9313), due to the separation of two electron withdrawing groups.

In addition, the auxiliary accepter benzoxazole in dyes **AZ6-B20** and **AZ6-B21** was almost coplanar with the adjacent thienyl unit, which was beneficial to the ICT effect. Compared with **AZ6**, the structures slightly twisted between the two thienyl groups in the dye **AZ6-B21**, in agreement with a blue-shift of the absorption spectra in a solution. The energy level band gap of the dye **AZ6-B21** and its twist angles between each part are close to **AZ6**, which may be the reason why its conversion efficiency is similar to **AZ6**.

3.5. DSSC performance

The IPCE spectra and J-V curves for DSSCs based on the three dyes are shown in Fig. 10, and the photovoltaic performance data are summarized in Table 5. The DSSCs based on **AZ6** produced a short circuit photo-current density (J_{sc}) of 16.32 mA cm^{-2}, an open circuit voltage (V_{oc}) of 698.96 mV, and a fill factor (*FF*) of 70.52%, corresponding to a PCE of 8.05%. In the same condition, inserting the benzoxazole group between the bithiophene and the acceptor cyoacetic acid, **AZ6-B21** based DSSCs provided J_{sc} of 13.92 mA cm^{-2}, V_{oc} of 749.46 mV, and *FF* of 78.76%, corresponding to a PCE of 8.22%. It is obvious that V_{oc} and *FF* increased in comparison with that for DSSCs based on **AZ6**. The high V_{oc} and *FF* of **AZ6-B21** lead to a high power conversion efficiency. Compared with **AZ6-B21**, DSSCs based on **AZ6-B20** preduced J_{sc} of 12.96 mA cm^{-2}, V_{oc} of 750.04 mV, and *FF* of 71.93%, possessing a low PCE of 6.99%. By comparison of **AZ6-B21** with **AZ6-B20**, **AZ6-B19** provided a smallest J_{sc} of 7.02 mA cm^{-2}, V_{oc} of 601.78 mV and a lowest PCE of 3.19%, such a dramatic decrease of PCE is probably resulted from the dipole moment separation by the insertion of the benzoxazole unit at the different site of the molecules.

The IPCE value of DSSCs based on **AZ6-B21** reaches the highest value of 83.45% at 495 nm, **AZ6-B20**, **AZ6** and **AZ6-B19** display the maximum IPCE values of 79.43% at 465 nm, 76.78% at 495 nm and 56.94% at 363 nm, respectively. The variation trend of IPCE spectra is consistent with the PCE of DSSCs.

To verify the intermolecular π-π stacking or aggregation of the dyes **AZ6-B21** and **AZ6-B20**, we added different concentrations multiples of chenodeoxycholic acid (CDCA) [6 CDCA (2.4 mM) and 8 CDCA (3.2 mM)] to dye sensitized solutions. The absorption spectra are shown in Fig. 11, the J-V curves and IPCE spectra for DSSCs are shown in Fig. 12 and Fig. 13 respectively, and the corresponding photovoltaic performance data are summarized in Table 6. The absorption range of the three sensitizers does not change much before and after the doping CDCA in the solution, but their absorption intensity decreases, which indicates that the photocurrent of the devices may decrease after co-adsorption [36]. The PCEs of the DSSCs after co-adsorption of CDCA (**AZ6-B20**: 7.48%, **AZ6-B21**: 8.67%, **AZ6-B19**: 3.27%), indicate that although the agglomeration of dye molecules is not serious, the recombination of charge with the electrons at the interfaces of TiO_2/-dye/electrolyte is improved.

3.6. Electrochemical impedance spectroscopy

To assess the electronic recombination rate and the electron lifetime, electrochemical impedance spectroscopy (EIS) was investigated. The Nyquist plot, Bode plot and Equivalent circuit model are shown in Fig. 14. In the Nyquist plot, there are two semicircles, and the larger

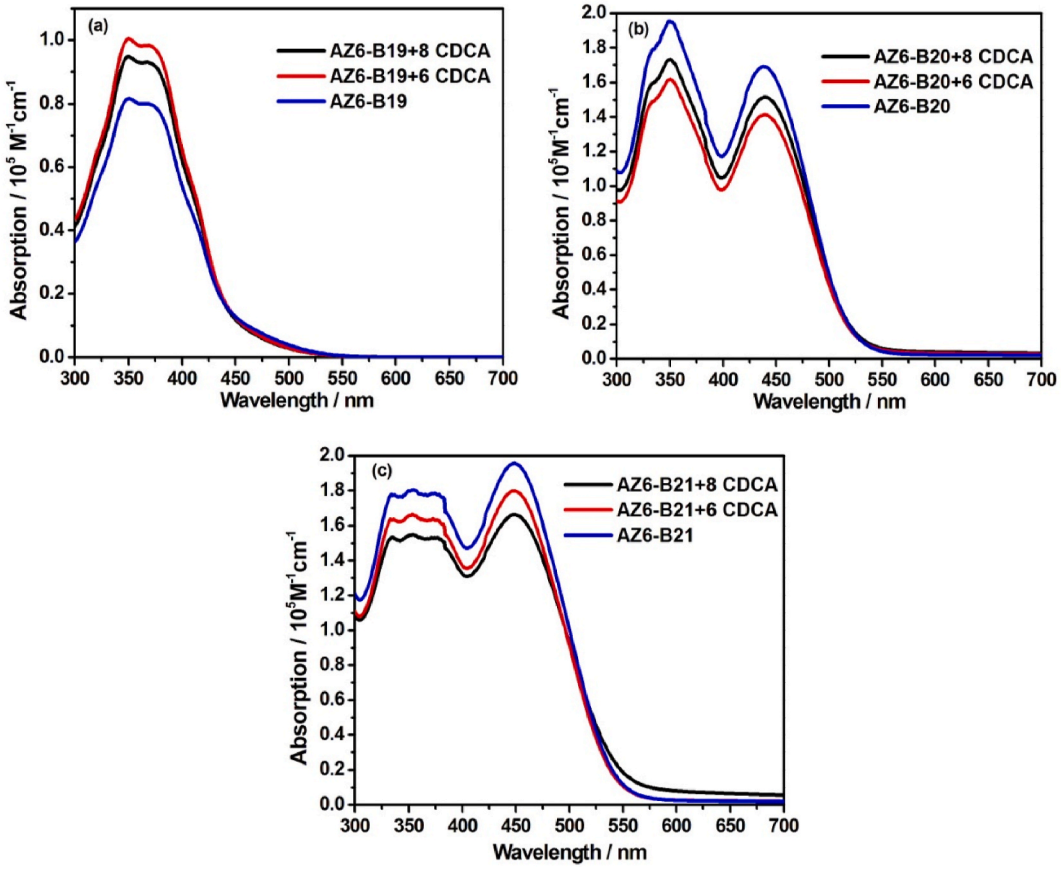

Fig. 11. The absorption spectra of (a) **AZ6-B19**, (b) **AZ6-B20** and (c) **AZ6-B21** in the solution with CDCA.

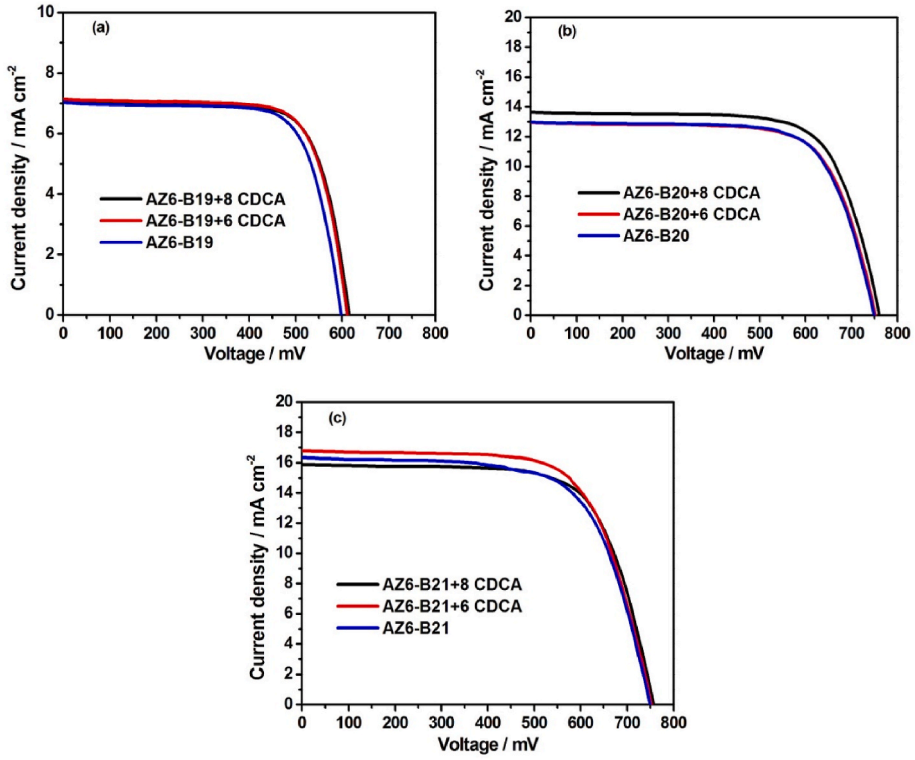

Fig. 12. *J-V* characteristics based on (a) **AZ6-B19**, (b) **AZ6-B20** and (c) **AZ6-B21** with CDCA.

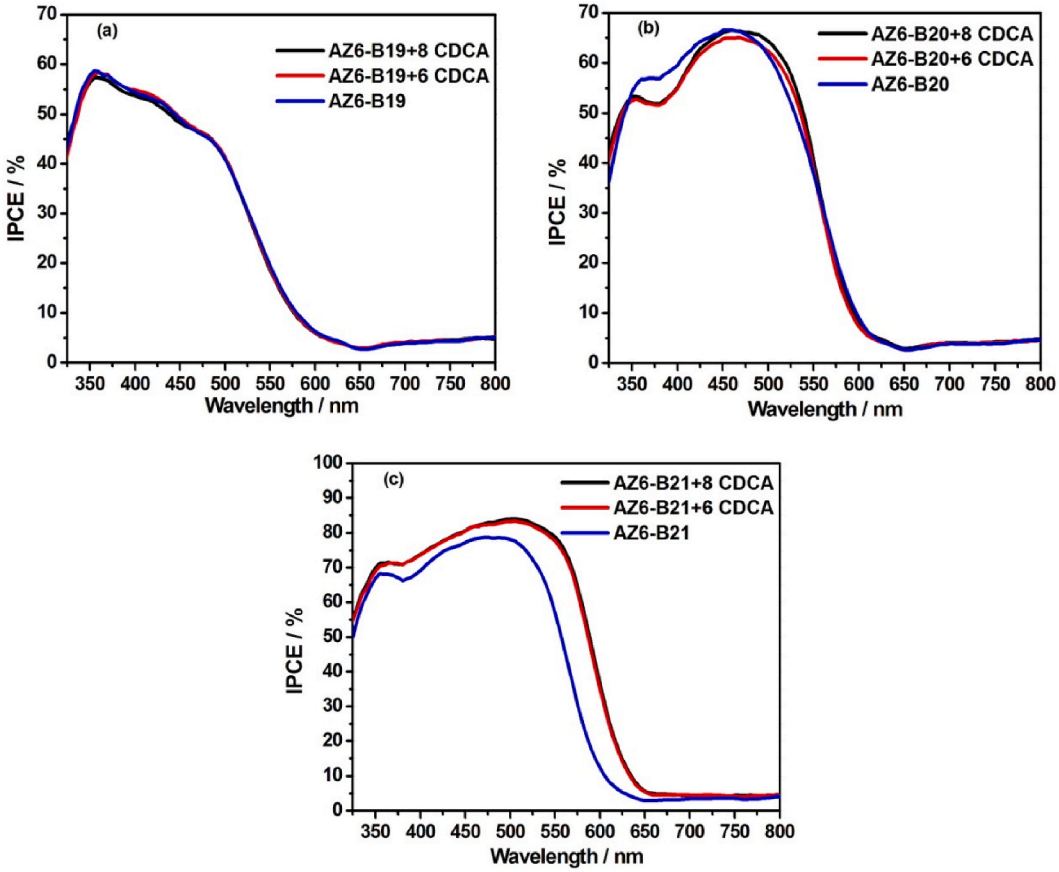

Fig. 13. IPCE spectra based on (a) **AZ6-B19**, (b) **AZ6-B20** and (c) **AZ6-B21** with CDCA.

Table 6
The photovoltaic performance data of the dyes with CDCA.

Dye	CDCA/ mM	J_{sc}/mA cm^{-2}	V_{oc}/ mV	*FF*	PCE/ %	IPCE/%(λ_{max}/ nm)
AZ6-B20	0	12.96	750.0	0.72	6.99	66.74(460)
AZ6-B20	2.4	10.62	754.3	0.88	7.01	65.75(460)
AZ6-B20	3.2	11.59	763.6	0.85	7.48	67.23(460)
AZ6-B21	0	13.92	749.5	0.79	8.22	78.90(495)
AZ6-B21	2.4	14.88	753.1	0.77	8.67	84.12(495)
AZ6-B21	3.2	15.87	757.5	0.70	8.41	84.51(495)
AZ6-B19	0	7.02	601.8	0.76	3.19	56.94(363)
AZ6-B19	2.4	7.12	611.5	0.75	3.27	59.72(360)
AZ6-B19	3.2	7.03	616.9	0.75	3.27	58.50(360)

semicircle at the intermediated frequency is assigned to the charge transfer impedance at the TiO_2/dye/electrolyte interface. The larger the radius of semicircle is, the greater the charge transfer resistance and the slower the electron recombination rate are obtained. The order of increasing radius is **AZ6-B19** < **AZ6** < **AZ6-B21** < **AZ6-B20**, referring to the electron recombination rate increase in the order of **AZ6-B20** < **AZ6-B21** < **AZ6**< **AZ6-B19**. In the Bode plot, the low frequency peak indicates the charge transfer process that electron injected in TiO_2 conduction band. The electron lifetime (τ_e) can be calculated from the peak frequency (*f*) in the low frequency range by the formulas of $\tau_e = 1/(2\pi f)$, the increasing order of electron lifetime is **AZ6-B19** (27.14 ms) <**AZ6** (27.14 ms) < **AZ6-B21** (37.98 ms) < **AZ6-B20** (38.08 ms). Obviously, the electron lifetime of **AZ6-B20** and **AZ6-B21** is significantly improved compared with **AZ6** due to the insertion of benzoxazole group in the molecule. It also means that the electron recombination between the injected electron and the electrolyte is effectively suppressed. Based on the data, the electron recombination rate and electron lifetime are consistent with the open circuit voltage.

3.7. Capacity

As shown in Fig. 7, the absorption peak strength of the dyes increases with the increase of dye solution concentration. The order of calculated capacity is **AZ6-B19** (0.98×10^{-7} mol cm^{-2}) < **AZ6** (1.09×10^{-7} mol cm^{-2}) < **AZ6-B20** (1.65×10^{-7} mol cm^{-2}) < **AZ6-B21** (1.82×10^{-7} mol cm^{-2}). The capacity of **AZ6-B21** and **AZ6-B20** are more than that of the others, which indicated that more dye molecules adsorbed in the TiO_2 films and also improved open circuit voltage (V_{oc}) and filling factor (*FF*) of **AZ6-B21** and **AZ6-B20** compared with dye **AZ6**.

4. Conclusion

In summary, two novel D-π-A-A sensitizers were synthesized by inserting the benzoxazole group as an auxiliary acceptor. The D-π-A-A dye sensitizers show much more intensive absorption of the sunlight but the band ranges are not as wide as that of the dye **AZ6** (without inserting benzoxazole unit). These dyes also provide much better adsorptive ability on the TiO_2 film and thereby to improve their photovoltaic performance (PCE of **AZ6-B21** is 8.22%). The high PCE (8.67%) of **AZ6-B21** based DSSCs can be further obtained by the co-adsorption of CDCA. On the other hand, the dye sensitizer D-A-π-A (**AZ6-B19**) is not as good as

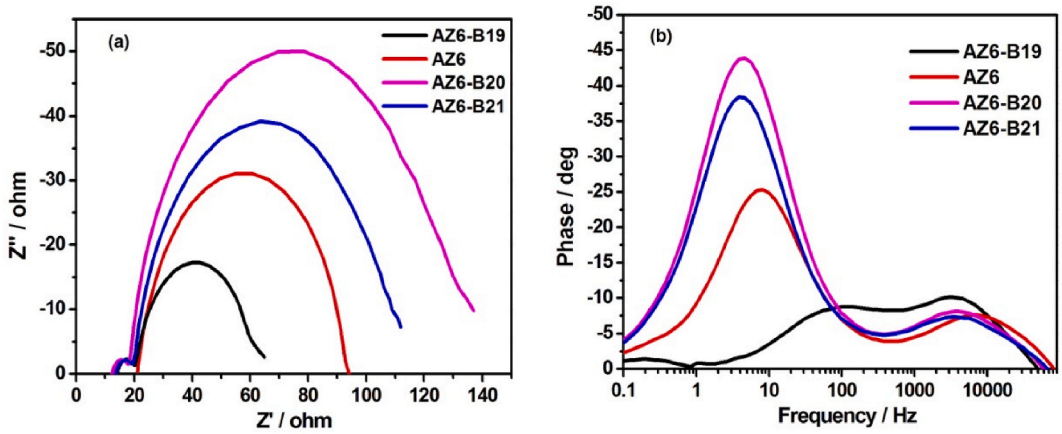

Fig. 14. EIS spectra of DSSCs at −0.7 V forward bias in the dark: (a) Nyquist and (b) Bode phase pots.

expected both for the light absorption and the photovoltaic performance (PCE of **AZ6-B19** is 3.19%). We speculate that the decrease of the dipole moment by the isolating the electron withdrawing groups is responsible for the declination.

Author statement

Methodology, S. Liu and M. Zhou; writing—original draft preparation, S. Liu and R. Chen; Synthesis of organic dyes, S. Liu and G. Zhang; Performance analysis, P. Zhou; Theoretical calculation, R. Chen; reference preparation, Q. An; writing—review and editing, Z. An, X. Chen and P. Chen; supervision, Z. An. The authors in our revised manuscript have agreed to publish this work in Dyes and Pigments.

Declaration of competing interest

The authors declare that they have no known competing financial interests or personal relationships that could have appeared to influence the work reported in this paper.

Acknowledgments

We are grateful to Professor Wenliang Wang at Shaanxi Normal University for theoretical calculations. Research was supported by National Science Foundation Committee of China (21673134), Program for Science & Technology Innovation Team of Shaanxi Province (2018TD-030).

Appendix A. Supplementary data

Supplementary data to this article can be found online at https://doi.org/10.1016/j.dyepig.2020.109093.

References

[1] Zhang B, Sun L. Artificial photosynthesis: opportunities and challenges of molecular catalysts. Chem Soc Rev 2019;48:2216–64.
[2] Song X, Yang X, Wang H, et al. Improving energy transfer efficiency of dye-sensitized solar cell by fine tuning of dye planarity. Sol Energy 2019;187:274–80.
[3] Joana MDC, Gabriel G, Francisco MF, et al. Influence of the meso-substituents of zinc porphyrins in dye-sensitized solar cell efficiency with improved performance under short periods of white light illumination. Dyes Pigments 2020;177:108280.
[4] Xu H, Zhu G, Jin Z. Electron migration optimization through nanostructural control of hierarchical Fe_3O_4 based counter electrodes for high-performance dye-sensitized solar cells. J Electroanal Chem 2020;869:114214.
[5] Gong J, Sumathy K, Qiao Q, et al. Review on dye-sensitized solar cells (DSSCs): Advanced techniques and research trends. Renew Sustain Energy Rev 2017;68:234–46.
[6] Jia H-L, Li S-S, Peng Z-J, et al. Efficient phenothiazine-ruthenium sensitizers with high open-circuit voltage (V_{oc}) for high performance dye-sensitized solar cells. Dyes Pigments 2020;180:108454.
[7] O'Regan B, Grätzel M. A low-cost, high-efficiency solar cell based on dye-sensitized colloidal TiO_2 films. Nature 1991;353:737–40.
[8] Kakiage K, Aoyama Y, Yano T, et al. Highly-efficient dye-sensitized solar cells with collaborative sensitization by silyl-anchor and carboxy-anchor dyes. Chem Commun 2015;51(88):15894–7.
[9] Ye J-H, Cheng C-K, Lin J-Y, et al. Potential-controlled pulse electrochemical deposition of poly nanostructural two-dimensional molybdenum disulfide thin films as a counter electrode for dye-sensitized solar cells. Surf Coating Technol 2020;394:125855.
[10] Wen Y, Wu W, Li Y, et al. Thieno [2, 3-b] indole-based organic dyes for dye-sensitized solar cells: effect of π-linker on the performance of isolated dye and interface between dyes and TiO_2. Org Electron 2016;38:61–8.
[11] Gong J, Sumathy K, Qiao Q, et al. Review on dye-sensitized solar cells (DSSCs): Advanced techniques and research trends. Renew Sustain Energy Rev 2017;68:234–46.
[12] Paek S, Choi H, Kim C, et al. Efficient and stable panchromatic squaraine dyes for dye-sensitized solar cells. Chem Commun 2011;47:2874–6.
[13] Rho W-Y, Jeon H, Kim H-S, et al. Recent progress in dye-sensitized solar cells for improving efficiency: TiO_2 nanotube arrays in active layer. J Nanomater 2015;16:85.
[14] Sharma K, Sharma V, Sharma SS. Dye-sensitized solar cells: fundamentals and current Status. Nanoscale Res Lett 2018;13:381.
[15] Slimi A, Hachi M, Fitri A, et al. Effects of electron acceptor groups on triphenylamine-based dyes for dye-sensitized solar cells: theoretical investigation. J Photochem Photobiol, A 2020;398:112572.
[16] Ahmad MS, Pandeya AK, Rahim NA. Advancements in the development of TiO_2 photoanodes and its fabrication methods for dye sensitized solar cell (DSSC) applications. A review. Renew Sustain Energy Rev 2017;77:89–108.
[17] Xu Z, Gao S, Lu X, et al. Theoretical analysis of the absorption spectrum, electronic structure, excitation, and intramolecular electron transfer of D-A′- π-A porphyrin dyes for dye-sensitized solar cells. Phys Chem Chem Phys 2020;22:14846–56.
[18] Xie Y, Zhou H, Zhang S, et al. Influence of the auxiliary acceptor and π-bridge in triarylamine dyes on dye-sensitized solar cells. Photochem Photobiol Sci 2019;18:2042.
[19] Li W, Wu Y, Zhang Q, et al. D-A-π-A featured sensitizers bearing phthalimide and benzotriazole as auxiliary acceptor: effect on absorption and charge recombination dynamics in dye-sensitized solar cells. ACS Appl Mater Interfaces 2012;4:1822–30.
[20] Zhu W, Wu Y, Wang S, et al. Organic D-A-π-A solar cell sensitizers with improved stability and spectral response. Adv Funct Mater 2011;21:756–63.
[21] Gong X, Li G, Wu Y, et al. Enhancing the performance of polymer solar cells by using donor polymers carrying discretely distributed side chains. ACS Appl Mater Interfaces 2017;9:24020–6.
[22] Huang R-Y, Tsai W-H, Wen J-J, et al. Spiro [fluorene-9,9'-phenanthren]-10'-one as auxiliary acceptor of D-A-π-A dyes for dye-sensitized solar cells under one sun and indoor light. J Power Sources 2020;458:228063.
[23] Li S, Yang X, Zhang L, et al. Effect of fluorine substituents on benzothiadiazole-based D-π-A-π-A photosensitizers for dye-sensitized solar cells. RSC Adv 2020;10:9203–9.
[24] Lim D-S, Choi K, Hayati D, et al. Blue-colored dyes featuring a diketopyrrolopyrrole spacer for translucent dye-sensitized solar cells. Dyes Pigments 2020;173:107840.
[25] Xie Y, Zhou H, Zhang S, et al. Influence of the auxiliary acceptor and π-bridge in triarylamine dyes on dye-sensitized solar cells. Photochem Photobiol Sci 2019;18:2042.
[26] Hemavathi B, Jayadev V, Ramamurthy PC, et al. Variation of the donor and acceptor in D-A-π-A based cyanopyridine dyes and its effect on dye sensitized solar cells. New J Chem 2019;43:15673–80.
[27] Tian L, Zhang X, Xu X, et al. The planarization of side chain in carbazole sensitizer and its effect on optical, electrochemical, and interfacial charge transfer properties. Dyes Pigments 2020;174:108036.
[28] Wu Z, An Z, Chen X, et al. Cyclic thiourea/urea functionalized triphenylamine-based dyes for high-performance dye-sensitized solar cells. Org Lett 2013;15:1456–9.

[29] Zhang G. Synthesis and property of thiourea functionalized organic dyes with π-linkers containing many hetero atoms. Shaanxi: Shaanxi Normal University; 2015.
[30] Zhu S, An Z, Chen X, et al. Approach to tune short-circuit current and open-circuit voltage of dye-sensitized solar cells: π-linker modification and photoanode selection. RSC Adv 2014;4:42252–9.
[31] Tian Y, Ying X, Zhou C, et al. Novel organic dyes for dye-sensitized solar cells based on 1-(2-ethylhexyl)pyrrole as a π –bridge. Dyes Pigments 2020;182:108655.
[32] Gauthier S, Robin-Le Guen F, Wojcik L, et al. Comparative studies of new pyranylidene-based sensitizers bearing single or double anchoring groups for dye-sensitized solar cells. Sol Energy 2020;205:310–9.
[33] Venkateswararao A, Tyagi P, Thomas KRJ, et al. Organic dyes containing indolo [2,3-b]quinoxaline as a donor: synthesis, optical and photovoltaic properties. Tetrahedron 2014;70:6318–27.
[34] Sayama K, Tsukagoshi S, Hara K, et al. Photoelectrochemical properties of J aggregates of benzothiazole merocyanine dyes on a nanostructured TiO_2 film. J Phys Chem B 2002;106:1363–71.
[35] Etienne T, Chbibi L, Michaux C, et al. All-organic chromophores for dye-sensitized solar cells: a theoretical study on aggregation. Dyes Pigments 2014;101:203–11.
[36] Zhang H, Chen Z-E, Zang X-F, et al. Optimize the rigid auxiliary groups on the donor to achieve self-inhibiting aggregation of the sensitizers. Sol Energy 2020; 204:330–6.